Chemical Papers (2022) 76:1045–1061
https://doi.org/10.1007/s11696-021-01938-8

ORIGINAL PAPER

Improvement of the reactivity of triethyl phosphate and structural behavior of hydroxyapatite versus the synthesis conditions by sol–gel route

Malika Merzougui[1] · Fatima Zohra Mezahi[1] · Achour Dakhouche[2] · Djelel Kherifi[1] · Foudil Sahnoune[3,4]

Received: 19 June 2021 / Accepted: 12 October 2021 / Published online: 18 October 2021

Abstract

Hydroxyapatite (HA) is a biocompatible and bioactive material used as bone-substitute materials in both orthopedics and dentistry. This work is devoted to studying the synthesis of hydroxyapatite (HA) by sol–gel route using triethyl phosphate (TEP) and calcium nitrate tetrahydrate as calcium and phosphor precursors. In order to optimize the hydrolysis of TEP, each prepared solution was aged in a closed Teflon® container. Several factors were tested in order to improve the synthesis conditions of well-crystallized HA. The effect of aging time (4 h, 16 h, and 24 h), aging temperature (25 °C, 50 °C, 70 °C, and 90 °C) of the prepared solutions, and the type of solvents (ethanol and/or distilled water) were tested. All dried gels were calcined at 700 °C for 1 h. The obtained results showed that the crystallinity degree of hydroxyapatite increases with aging time and temperature, which must not exceed 70 °C. When the prepared solutions were aged at 90 °C, the tri-calcium phosphate (TCP) was formed as a major phase and HA was present as a very minor phase. It was remarked that the aging of sols in a closed Teflon container® leads to an important decrease of the aging time and temperature. It was found that 24 h and 70 °C are the optimal conditions for the synthesis of well-crystallized HA. Also, it was deduced that a sufficient amount of water was needed to hydrolyze the triethyl phosphate and consequently, to obtain a well-crystallized HA.

Keywords Sol–gel · Hydroxyapatite · Hydrolysis · Aging time · Aging temperature · Solvent

Introduction

Hydroxyapatite (HA: $Ca_{10}(PO_4)_6(OH)_2$) is based on calcium phosphate, which is the basic mineral component of human bones and teeth (Shi et al. 2009). Because of this similarity, several studies have focused on hydroxyapatite as one of the most important alternative biomaterials in orthopedics and dentistry (Glimsher 1984). HA advantages as a biomaterial include a good osteoconductivity, non-toxicity, and the ability to form a direct bond with bone (Rhee 2002). Also, HA is used as a sorbent in order to purify the wastewater by removing the heavy metals such as arsenic and cadmium (Kongsri et al. 2013).

HA can be prepared from natural materials such as coral or bones (Joschek et al. 2000; Mezahi et al. 2005, 2009). Besides, it can be synthesized in several ways such as the precipitation method (Andrasekhar et al. 2013; Kamalanathan et al. 2014), hydrothermal (Ji et al. 2015; Wu et al. 2013), and sol–gel route (Masuda et al. 1990; Gross et al. 1998a, b; Song et al. 2002; Fathi and Hanifi 2009; Vijayalakshmi and Rajeswari 2012; Mojahedian et al. 2016; Negrila et al. 2018; Shalini and Kumar 2019). These different methods affect the HA properties such as particle size, morphology and microstructure which determine the applications of HA into different fields (Ghosh et al. 2011; Padmanabhan et al. 2009). Accordingly, the medical applications favor the use of nano-crystalline HA that performs improved sinterability, mechanical properties such as fracture toughness, densification and bioactivity owing to larger surface

✉ Fatima Zohra Mezahi
fatimazohra.mezahi@univ-msila.dz

[1] Physics and Chemistry of Materials Laboratory, Department of Physics, Mohamed Boudiaf University, 28000 M'sila, Algeria

[2] Inorganic Materials Laboratory, Department of Chemistry, Mohamed Boudiaf University, 28000 M'sila, Algeria

[3] Department of Physics, Mohamed Boudiaf University, 28000 M'sila, Algeria

[4] Research Unit on Emerging Materials (RUEM), Ferhat Abbas University- Setif 01, 19000 Setif, Algeria

area (Kalita et al. 2007b). Moreover, the nano-crystalline HA can be used as a therapeutic agent carrier; it destroys and restrains the spread of cancer (Yang et al. 2012). It was reported that sol–gel route is an exceptional method designed for achieving an ultrafine powder (less than 10 nm in size). In addition, the sol–gel route has many advantages in comparison to the traditional ways (Webster et al. 2000), which are: low energetic cost, better chemical homogeneity, high purity, control of the condensation reactions, lower reaction temperature, and the possibility of producing new materials with different forms (Johnson et al. 1985). The sol–gel route allows the mixing of calcium and phosphorus precursors at the molecular level, which improves the chemical homogeneity of HA (Ferraz et al. 2004; Ishikawa and Kareiva 2020b). Also, the improvement of the conditions for synthesis of pure HA, such as the reaction temperature, pH, solvents, and concentration of reactants, are the key factors for getting controllable aspect ratios and bioactivity.

Ishikawa et al. (2020a; b) collected the most research works about the synthesis by sol–gel route of the hydroxyapatite with different shapes such as powders or thin films. In view of that, organic and inorganic precursors were used. For the first time in 1990, Masuda et al. (1990) used the alkoxides as starting materials for HA synthesis through the sol–gel technique. Also in 1998, Gross et al. 1998a, b) used calcium diethoxide and triethyl phosphate as starting precursors to prepare HA. But, just a few researchers continued using the pure alkoxides precursors for HA preparation by sol–gel route. Many authors recommended, for HA synthesis by sol–gel method, to only use inorganic precursors. In some works, phosphorous pentoxide (P_2O_5) and calcium nitrate tetrahydrate ($Ca(NO_3)_2.4H_2O$) were used as phosphorous and calcium sources (Song et al. 2002; Fathi and Hanifi 2009; Vijayalakshmi and Rajeswari 2012; Mojahedian et al. 2016). However, in various works, phosphorous pentoxide (P_2O_5) was replaced by ammonium hydrogen phosphates ($(NH_4)_2HPO_4$) as source of phosphorous (Negrila et al. 2018; Shalini and Kumar 2019). Or, phosphoric acid (H_3PO_4) and calcium acetate monohydrate ($Ca(CH_3COO)_2.H_2O$) were exploited by other researchers (Stankeviciūtė et al. 2013; Malakauskaitė -Petruleviciene et al. 2016; Jonauskė et al. 2019). Also, calcium chloride ($CaCl_2$) and sodium phosphate (Na_3PO_4) were chosen by Kheimehsari et al. (2015) for HA synthesis by sol–gel route. Generally, absolute ethanol was used to dissolve the raw materials. Sometimes the mixture of different solvents was used for the preparation of sols such as 2-butanol, ethanol, acetic acid, and water (Saranya et al. 2011; Mojahedian et al. 2016). Noted that, triethyl phosphate ($PO(OC_2H_5)_3$), triethyl phosphite ($P(OC_2H_5)_3$), and other alkyl phosphates were used as sources of phosphorus (Hsieh et al. 2001; Ben-Nissan et al. 2001; Liu et al. 2001, 2002; Chandanshive et al. 2013; Chen et al. 2011; Foroughi et al. 2015; Priyadarshini and Vijayalakshmi 2018); methyl, ethyl, and propyl-alcohol were used as solvents. Or, instead of calcium alkoxides, calcium nitrate ($Ca(NO_3)_2{\cdot}4H_2O$) was the most popular calcium precursor for the HA preparation (Hsieh et al. 2001; Ben-Nissan et al. 2001; Liu et al. 2001, 2002; Chandanshive et al. 2013). Nevertheless, in other works, the calcium acetate (Cihlar and Castkova 1984; Kordas and Trapalis 1997) was used to prepare HA. To hydrolyze triethyl phosphite, some authors used a mixture of anhydrous ethanol and distilled water (Vijayalakshmi and Rajeswari. 2006; Balamurugan et al. 2006; Eshtiagh-Hosseini et al. 2007). In other research, only distilled water with a fixed amount was used to hydrolyze the triethyl phosphite or triethyl phosphate (Kalita and Bhatt 2007a; Dinu et al. 2013). Calcium chloride ($CaCl_2{\cdot}2H_2O$) and calcium oxide (CaO) were also used as calcium sources in the similar sol–gel synthesis routes for HA (Ioitescu et al. 2009; Hosseini et al. 2017).

Generally, the time and temperature of gelling of the prepared solutions varied from study to another. Also, the time of aging of the prepared solutions varied from 2 to 72 h. But in most of the works, the ambient temperature was used as the temperature of aging of the prepared solutions. In this work, the precursors calcium nitrate tetrahydrate $Ca(NO_3)_2.4H_2O$ and triethyl phosphate ($PO(C_2H_5O)_3$, TEP) are selected as sources of Ca and P. TEP is chosen because it remains relatively stable despite to triethyl phosphite (Bilton et al. 2010). Nevertheless, it is reported that triethyl phosphate has a relatively low reactivity for hydrolysis. Also, long aging times (several days) and high solution temperatures are needed (Liu et al. 2001; Qiu et al. 1993; Westheimer et al.1988).

In order to optimize the hydrolysis of TEP, the aging of the prepared solutions will be done in a closed Teflon® container at a determined temperature. Accordingly, the aim of this work is to optimize the hydrolysis of TEP in order to determine the optimal conditions for HA synthesis by sol–gel route. So, the effect of aging conditions (time and temperature) of the prepared solutions on HA synthesis was evaluated. The distilled water and/or ethanol were also tested as solvent medium in order to obtain well-crystallized HA.

Experimental section

Materials and method of synthesis

In order to obtain pure hydroxyapatite, two-based precursors were used as sources of calcium and phosphorus ions, respectively: calcium nitrate tetrahydrate ($Ca(NO_3)_2,4H_2O$, Biochem, 98%) and triethyl phosphate (TEP: $C_6H_{15}O_4P$, Aldrich, 99%). The distilled water and/or anhydrous ethanol (C_2H_5OH) were chosen as the medium solvent.

The two precursors were dissolved separately. 0.03 M of triethyl phosphate was diluted in 5 mL of medium solvent under vigorous magnetic stirring in order to obtain a transparent solution. On the other hand, 0.05 M of calcium nitrate tetrahydrate was dissolved in 25 mL of medium solvent, the molar ratio of precursors is Ca/P = 1.67, which is the stoichiometric molar ratio in HA. After that, the calcium nitrate solution was added drop wise to the stirred phosphorus solution. The vigorous stirring of the mixing solutions continued for a further 30 min. Renowned for that, each prepared solution was aged in a closed cylindrical Teflon® container. After that, a slow evaporation was done in an open container, generally at 70 °C for 1 day in order to obtain gel. The obtained gels were dried for 1 day at 70 °C.

In order to obtain well-crystallized hydroxyapatite, many assays were performed to determine the optimal conditions for HA synthesis (Fig. 1). Firstly, the effect of aging time (4, 16, and 24 h) was studied, 70 °C was chosen as the temperature of aging, gelling and drying. Secondly, the effect of aging temperature (25, 50, 70, and 90 °C) was tested. For this assay, the temperature of gelling and drying is fixed at 70 °C for 1 day. Or, for the 90 °C aging temperature, the temperature of gelling and drying is fixed at 90 °C. Finally, the effect of medium solvent (distiller water (DW) and/or ethanol (Eth)) was tested. According to the results of the first and the second assay, the temperature of aging, gelling and drying was fixed at 70 °C for 1 day. It is noted that the pH of the mixtures of solutions was measured at the end of the magnetic stirring and aging process. The dried gels were calcined at 700 °C for 1 h with 5 °C/min heating rate. The obtained powders were crushed into fine powder in order to do the analyses.

Characterization

X-ray diffraction (XRD) was employed to investigate the crystalline phases present in the calcined powders by using X'PERT PRO diffractometer operating at 40 kV and 30 mA. The data were collected over a range of 10°–60° in 2Θ with a step size of 0.016° and a time per step of 0.5 °C/sec. The degree of HA crystallinity, expressed as the fraction of the crystalline phase, was estimated from the XRD data using the following equation (Pang and Bao 2003):

$$\mathbf{X_c} = 1 - \left(\frac{\mathbf{V}_{(112/300)}}{\mathbf{I}_{(300)}}\right) \quad (1)$$

I_{300}: intensity of the (300) peak, $V_{112/300}$: intensity of the hollow between the (112) and (300) diffraction peaks, where 112 and 300 are the corresponding hkl miller indices of the peaks.

Also, the Ca/P molar ratio in the prepared powders was calculated using X-ray Fluorescence (XRF) (Shimadzu, Japan). However, the average crystallite size (D) of HA was estimated using Scherrer's formula (Jenkins and Snyder 1996):

$$\boldsymbol{D} = \frac{0.9\lambda}{\boldsymbol{FWHM cos\theta}} \quad (2)$$

λ is Cu K_α wavelength 1.5406 A°, and FWHM is the full width at half maximum for the diffraction peak (rad) and θ is the diffraction angle (°). Three diffraction peaks (002), (211), and (222), situated, respectively at 25.8°, 31.75°, and 46.7°, were chosen for calculation of the crystallite size.

Furthermore, Fourier-transform infrared spectroscopy (FTIR) was used to analyze the functional group of existent

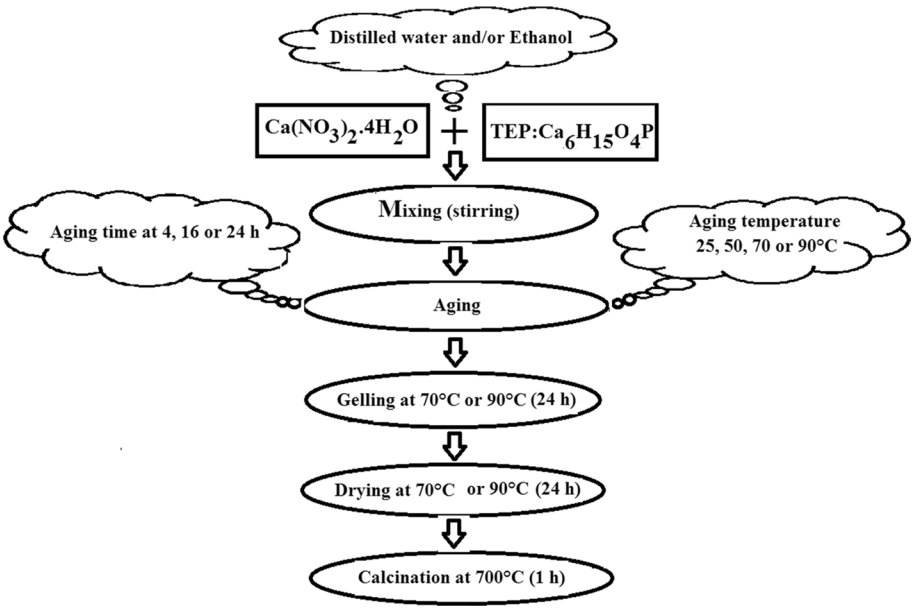

Fig. 1 Flow chart of HA synthesis by sol–gel route

phases in the synthesized powders. The measurements were carried out in the transmission mode in the mid-infrared range (400–4000 cm^{-1}), with a resolution of 4 cm^{-1}. 2% of the powder was mixed with 98% dried KBr. The analyses were performed using the JASCO FTIR – 4200 spectrometer. In addition, the thermal behavior of the powders was studied by thermal gravimetric analysis (TGA), using a SETARAM equipment (LABSYS EVO DTA/DSC-TG) in the 25–1000 °C temperature range with a heating rate of 20 °C min^{-1}, Ar environment and Al_2O_3 reference. The scanning electron microscopy (SEM) TESCAN VEGA3 was used to evaluate the morphology of the prepared HA powders. In addition, the particle size distribution of the prepared powders was measured using a laser scattering particle size distribution analyzer (Horiba, LA-960).

Results and discussion

Effect of aging time on HA synthesis

As described for the synthesis steps elsewhere, in this assay, both TEP and calcium nitrate tetrahydrate were dissolved in distilled water; a clear solution was obtained at the end of the magnetic stirring. The prepared solutions were aged at 70 °C for different times: 4, 16 and 24 h in a closed Teflon® container. After that, the solutions were sealed in a glass beaker and kept at 70 °C for 1 day in order to obtain a gel. Further drying of the obtained gel, at 70 °C for 1 day, led to a white powder. The dried gel was crushed into a fine powder and calcined at 700 °C for 1 h with 5 °C/min heating rate. It was remarked that just after approximately 3/4 of the solvent was removed at 70 °C, the prepared sol transformed into a clear and viscous liquid. A continued heating of viscous sol at 70 °C resulted in a white solid gel.

As shown in Table 1, pH values of the prepared solutions decrease with aging time from 5.68 value at end of stirring to zero value after 24 h aging time. The decay of pH solutions proofs the hydrolysis of TEP. Renowned for that, the resulted products of hydrolysis form a complex with the calcium ions dissolved in the solution during aging. The hydrolyzed phosphorus sol interacts with the Ca sol, in the form of Ca^{2+} ions in water, to form oligomeric derivatives containing Ca-O-P bonds. According to the hydrolysis reaction of triethyl phosphate described by Anjaneyulu et al. (2016), the aqueous-based process of triethyl phosphate may proceed as follows:

$$\begin{aligned}&\mathbf{PO(OEt)_{3-x}(OH)_x + Ca^{2+} + NO_3^-}\\&\quad\rightarrow \mathbf{\left(NO_3^-\right) - (OH) - Ca - O - PHO(OEt)_{3-x'}}\\&\qquad\mathbf{+ H^+ + C_2H_5OH + H_2O}\end{aligned} \tag{3}$$

The release of the protons has led to a decrease in the pH of the prepared solutions mainly in the first hours of the aging time. If the heating operation continued, the solvents would be removed. Consequently, the thermal dehydration accelerated and the polymerization occurred. Hence, the condensation between these derivative units results in the formation of further (-Ca-O-P-) bonds in the dry gels (Beganskienė et al. 2003).

XRD patterns of synthesized and calcined powders as a function of aging time (Fig. 2) illustrate the formation of crystalline hydroxyapatite (pdf # 00-009-0432) for all aging times. Also, calcium oxide CaO (pdf # 01-077-2376) is present as the second phase. The superposition of CaO and HA peak at 32.1° 2θ leads to obtaining a broadening peak with higher intensity. As justified by other researchers, the presence of CaO is the result of decomposition of calcium nitrate unreacted with TEP in the gel and caused by the phosphorus volatilization (Fathi et al. 2008). Different studies showed that sol–gel derived HA is always formed together with a second phase. Many of these studies showed the formation

Table 1 pH values of prepared solutions, crystallite size, crystallinity and molar ratio (Ca/P) for the prepared powders versus the aging time

Aging time (h)	pH	Crystallite size (nm)	Crystallinity (%)	Molar ratio Ca/P
0	5.68	–	–	–
4	1.50	48.58	81	3.36
16	0.15	56.20	90	2.73
24	0	58.54	93	1.97

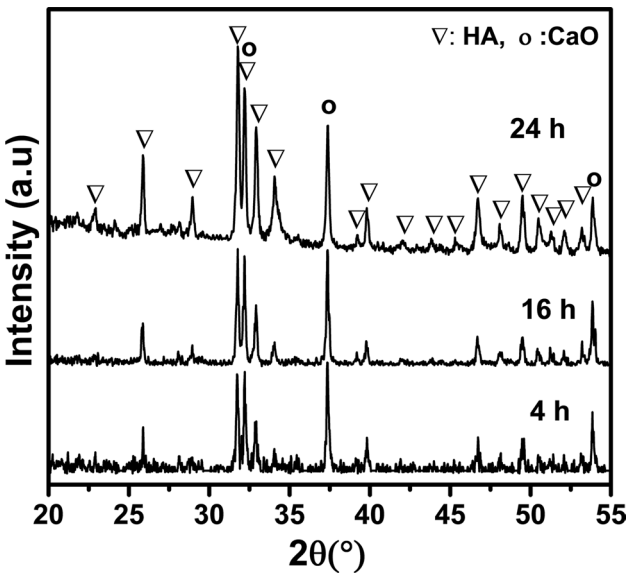

Fig. 2 XRD patterns of prepared powders versus the aging time, calcined at 700 °C

of CaO as a second phase (Chung et al. 2005; Liu et al. 2002; Pang 2003; Santos et al. 2015). Or, other researchers showed the formation of β-TCP together with or without CaO as second phases (Bakan et al. 2013; Chandanshive et al. 2013; Fathi and Hanifi 2009; Green et al. 1999). Moreover, other studies established the formation of $CaCO_3$ as second phase together with HA (Anjaneyulu et al. 2016; Vijayalakshmi and Rajeswari 2012).

It was remarked that HA peaks are dominant peaks and their intensities increase in contrast to that of CaO peaks with aging time. In addition, the width of the peaks becomes narrower. So, these results are a sign of an increase in the crystallinity degree and the crystallite size with aging time. The values of the crystallinity degree and the crystallite size confirm this suggestion (Table 1). Also, it can be observed that the value of the Ca/P molar ratio (Table 1); in all prepared powders; was superior to that of the stoichiometric molar ratio in HA. This can be justified by the presence of the second phase CaO as shown by XR patterns. Or, the calculated Ca/P molar ratio decreased (from 3.36 to 1.97) with the aging time and moved toward the stoichiometric molar ratio in HA for 24 h aging time. As mentioned previously, the amount of CaO decreased with aging time, which leads, consequently, to the decrease of the Ca/P molar ratio.

Figure 3 shows infrared (FTIR) results for synthesized powders at different aging times and treated at 700 °C. The results confirm the presence of phosphate, hydroxide and carbonate groups for all aging times. The phosphate groups (PO_4^{3-}) are proved by the apparition of P-O stretching modes at 1093, 1044 (υ_3) and 959 cm^{-1} (υ_1); and the O–P–O bending modes located at 604, 568 (υ_4) and 468 cm^{-1} (υ_2). Moreover, the two bands at 3573 and 639 cm^{-1} attested the presence of the stretching and bending modes of hydroxyl groups (OH^-) (Koutsopoulos 2002; Joris and Amberg 1971). While the two peaks at 1414 and 1464 cm^{-1} indicate the presence of the carbonate group. The peak located at 879 cm^{-1} can be assigned to the carbonate group or to the (HPO_4) group characteristic of deficient HA. It is known that there are two sites for the incorporation of carbonate ions in hydroxyapatite crystals: site A (OH^- site) and site B (PO_4^{3-} site) (Vignoles et al. 1989). The peaks at 1993.8–2094 cm^{-1} are the overtone and combination bands of PO_4^{3-} ions (Joris and Amberg 1971). An additional narrow peak was observed at 3640 cm^{-1}, which is assigned to the stretching mode of O–H in $Ca(OH)_2$. It can justify the presence of $Ca(OH)_2$ that calcium oxide is unstable at ambient conditions and at high temperatures because of its tendency to react with atmospheric moisture to form more stable compounds such as calcium hydroxide ($Ca(OH)_2$) (Suchanek and Yoshimura 1998). This phase was not identified by XRD analysis because their first higher peaks have the same 2θ values as any HA peaks. It is noticeable that the two bands at 1644 and around 3400 cm^{-1} are due to the adsorbed molecular water (Koutsopoulos 2002). It can be observed that the intensity of the characteristic bands of HA increased and became narrower, or that of $Ca(OH)_2$ decreased with the increasing of the aging time. This is in good accordance with the XRD analysis. So, the crystallinity of HA increases with aging.

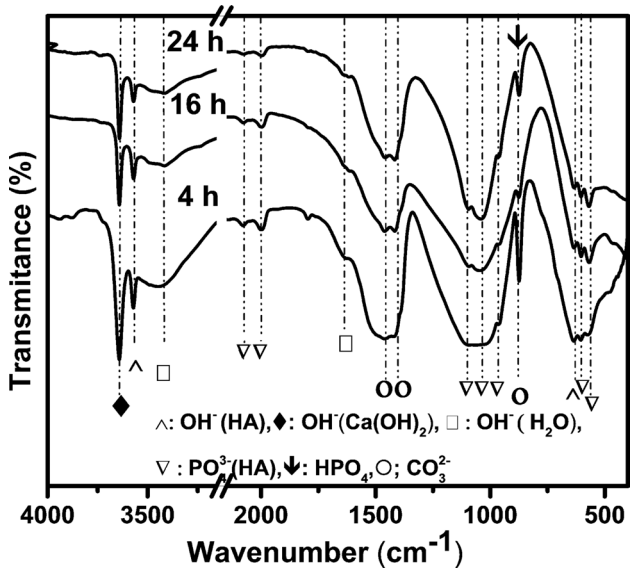

Fig. 3 FTIR spectra of prepared powders versus the aging time, calcined at 700 °C

The decomposition temperature strongly depends on the synthesis technique of the HA powder. As presented in Fig. 4, TG-DSC curves exhibit the same trend for the two aging times 4 and 24 h. Both of the samples showed four weight-loss stages such as 30–150 °C, 150–350 °C, 350-500 °C, and 500–650 °C. No supplementary weight loss was distinguished from 650 °C. The first week weight loss corresponds to the departure of the volatile products resulting from the hydrolysis of TEP, such as ethanol and adsorbed water still trapped in the dry gel. In the second stage, the weight loss is significant. It corresponds to the departure of structural water resultant from the dehydration of nitrates and the pyrolysis processes of organic compounds justified by the apparition of the endothermic peak at ~ 185 °C and exothermic peak at 284 °C. XR pattern of the gel treated at 300 °C for 24 h aging time (not shown in this work) illustrated the presence of a mixture of calcium nitrates and calcium nitrate tetrahydrate. Also, $CaCO_3$ and CaO were present as minor phases. According to Vijayalakshmi and Rajeswari (2012), the formation of carbonate groups is due to the presence of ethyl radicals in the dried powder, which arises from the TEP precursor. They showed that $CaCO_3$ was present as a main second phase together with HA in the dried gel treated at 300 °C. At the third stage, the weight loss is very low. The exothermic peak at 385 °C for 4 h aging

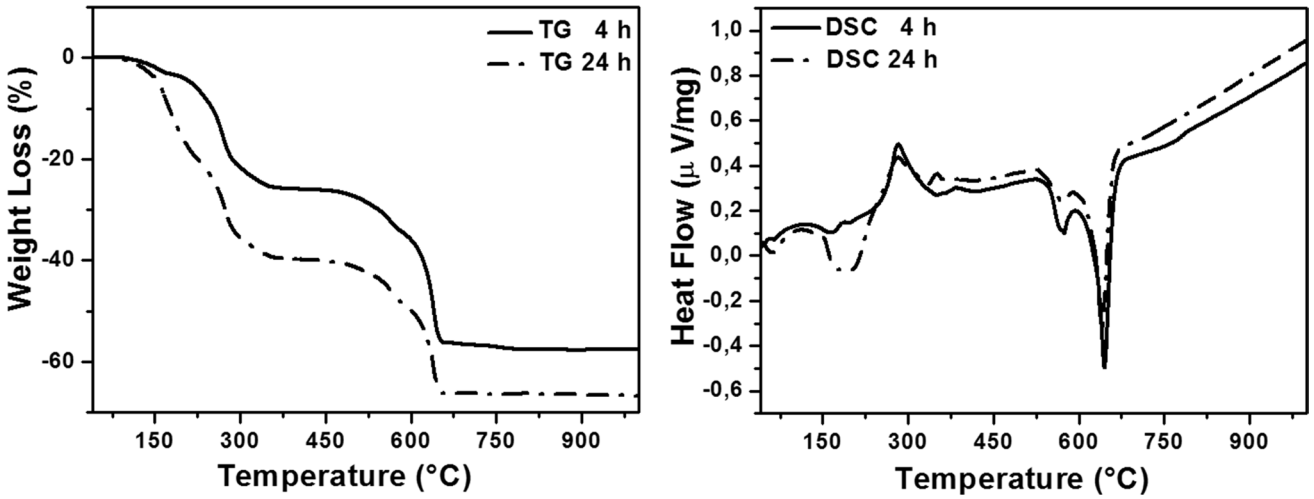

Fig. 4 TG-DSC curves of prepared powders, versus the aging time, calcined at 700 °C

time and 352 °C for 24 h aging time correspond to the crystallization temperature of hydroxyapatite in the two samples. XR pattern of the gel treated at 300 °C for 24 h aging time (not shown in this work) confirms the HA crystallization. Also in the fourth stage, the weight loss is significant. Two endothermic peaks appeared around 572 and 640 °C for 4 and 24 h aging time, respectively. The first peak presents the melting temperature of calcium nitrate. Or, the second peak corresponds to the liquid solution decomposition into calcium oxide, nitrogen dioxide, and oxygen (Vollmer and Ayers 2012; Yuvaraj et al. 2003). Noted that, the XR patterns of the gel treated at 700 °C confirmed the disappearance of peaks characteristic of calcium nitrates, CaO peaks only were present. Calcium nitrates dehydration and decomposition occur according to the following reactions (Yuvaraj et al. 2003):

$$\mathbf{Ca(NO_3)_2, 4H_2O \rightarrow Ca(NO_3)_2 + 4H_2O} \tag{4}$$

$$\mathbf{Ca(NO_3)_2 \rightarrow CaO + 2NO_2 + \frac{1}{2}O_2} \tag{5}$$

There are many works that have studied the effect of aging time on the formation of hydroxyapatite (Gross et al. 1998a, b; Fathi and Hanifi 2009; Liu et al. 2002; Beganskienė et al. 2003; Green et al. 1999; Bakan et al. 2013; Tredwin et al. 2009). But, just a few works used thermal analysis in order to study this effect. According to the thermal analysis results obtained by Fathi and Hanifi (2009) and Liu et al. (2002), the insufficient aging leads to excessive weight loss upon calcinations. Nevertheless, the obtained results show that the weight loss ratio upon calcinations decreases with the decrease in aging time. The TG results illustrate that the total weight loss of the sample with 4 h aging time (57%) is less by approximately 10% of the sample with 24 h aging time (67%). Fathi and Hanifi (2009) used phosphoric pentoxide (P_2O_5), calcium nitrate tetrahydrate, and absolute ethanol to prepare nano-hydroxyapatite. Liu et al. (2002) used triethyl phosphite, calcium nitrate tetrahydrate, and distilled water to prepare nano-hydroxyapatite. The difference in the type of the used precursors, solvent and synthesis protocol may have led to the dissimilarity of hydrolysis and poly-condensation processes and consequently the weight loss ratio. Also in the current study, the difference in weight loss started at the first heating stage. So, the gel with a complete hydrolysis of TEP and more formation of P–O–Ca bond contains a greater amount of residual water and consequently the more weight loss occurs. Also, the weight loss difference continued during the pyrolysis of organic compounds, which leads to conclusion that the organic compounds are more present in the gel aged for 24 h.

Figures 5 and 6 illustrate the size distribution and micrographs of the powders versus the aging time. For all powders, a mixture between agglomerates and fine particles was observed with a bimodal distribution. Generally, the size distribution of the fine particles fluctuates between 0.05 and 0.5 μm. Or, the second distribution varies between 0.6 and 16 μm. However, for 4 h aging time, the powder comprises minor fine particles and tended to agglomerate strongly in comparison to other times. Also, the maximum frequency decreases with aging time from 5.12 to 3.41 μm (D_{50} = 4.39 μm, D_{90} = 7.15 μm (4 h)/D_{50} = 2.52 μm, D_{90} = 5 μm (24 h)). The results of the size distribution are in well accordance with the micrographs. As the aging time increases, the size of the agglomerates decreases and also their shape becomes more homogeneous (also spherical indeed the elongated shape). Certainly, the decrease in grain

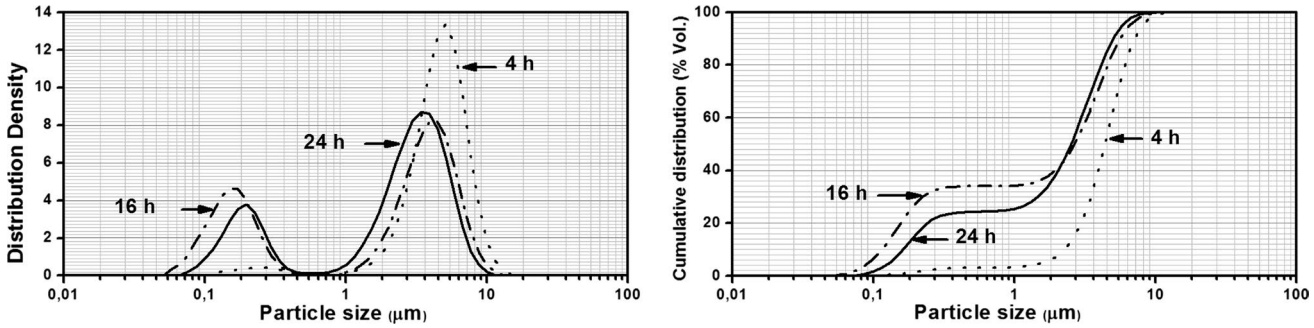

Fig. 5 Particle size distribution of prepared powders, versus the aging time, calcined at 700 °C

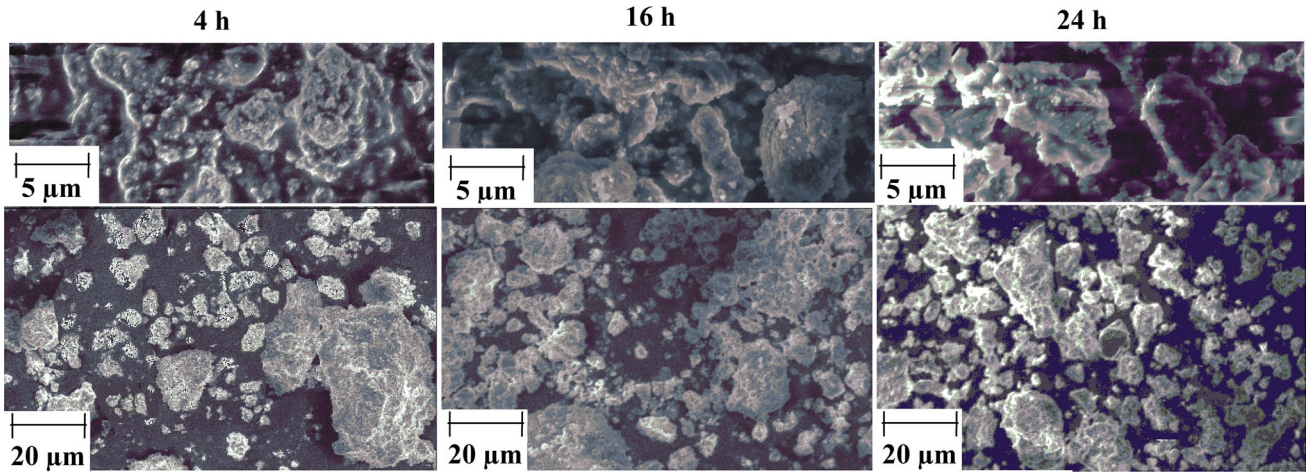

Fig. 6 SEM micrographs of prepared powders, versus the aging time, calcined at 700 °C

size leads to the further agglomeration of particles and consequently the increase in the agglomerates size.

According to the obtained results, the aging time plays an important role in the formation of well-crystallized hydroxyapatite particles. As the aging time increases, the pH values decrease which improves the hydrolysis of TEP and, consequently, the condensation of the resulted products with the calcium ions dissolved in the solution during aging. Thus, the increase in aging time leads to the formation of further (-Ca-O-P-) bonds in the dry gels (Beganskienė et al. 2003). As a consequence, the cross-linked structure of the molecules increases and favors the formation of large crystallite of well-crystallized HA (Fathi and Hanifi 2009; Balamurugan et al. 2006; Santos et al. 2015).

It can be suggested that the aging time (24 h) is the needed time required for the hydrolysis of all of TEP and the combination of phosphorous and calcium precursors, which leads to more crystallized and stable HA.

Effect of aging temperature on HA synthesis

In this assay, each one of TEP and calcium nitrate was diluted in distilled water and mixed as demonstrated previously; a clear solution was obtained at the end of the magnetic stirring. The prepared solutions were aged at different temperatures 25, 50, 70 and 90 °C for 1 day in the closed Teflon® container. After that, the solutions were kept at 70 °C for 1 day in order to obtain gel. Nevertheless, for 90 °C aging temperature, the temperature of gelling and drying was also 90 °C. The further drying of gel at 70 °C (or 90 °C) for 1 day leads to get white powder. The dried gel was crushed to fine powder and calcined at 700 °C for 1 h with 5 °C/min heating rate.

The pH values of the HA solutions versus the aging temperatures (25, 50, 70, and 90 °C) are shown in Table 2. At the end of the magnetic stirring, the pH value of the prepared solution was 5.35. After that, the pH decreased after one day of aging time with aging temperature. For 90 °C aging temperature, pH was not measured because the gelling process was not observed and the evaporation of the solution was

Table 2 pH values of prepared solutions, crystallite size, crystallinity, and molar ratio (Ca/P) for the prepared powders versus the aging temperature

Aging temperature (°C)	pH	Crystallite size (nm)	Crystallinity (%)	Molar ratio Ca/P
25	3.60	50.75	87	4.10
50	1.72	52.77	88	3.06
70	0	58.54	93	1.97
90	–	–	–	1.78

important. A white powder was obtained within one day of aging time. The hydrolysis of TEP was remarked entirely just for 70 °C aging temperature where the pH attends zero value contrary to the other temperatures.

Figure 7 shows XRD patterns of the prepared powders versus the aging temperature. The patterns reveal the formation of crystalline hydroxyapatite (pdf # 00-009-0432) as the major phase, together with CaO (pdf # 01-077-2376) as the second phase for temperatures 25, 50, and 70 °C. The peaks intensities of HA increase in contrast to that of CaO with aging temperature. Also, the width of HA peaks becomes narrower, which indicates an increase in the crystallinity degree. So, it can be concluded that temperature optimizes the hydrolysis and polymerization process and consequently, the HA crystallization until 70 °C.

Nevertheless, for 90 °C aging temperature, the intensity of HA peaks became very weak and another dominant phase appeared, which was identified as β-tricalcium phosphate phase (β-TCP, ICDD N° 9-0169). Moreover, $Ca(OH)_2$ (pdf # 01-084-1271) was present.

Kim et al. (2004) showed that ß-TCP forms as consequence of the fast reaction of the calcium nitrate with TEP. Furthermore, as demonstrated by Tredwin et al. (2009), the excess of the temperature more than 40 °C may cause the loss and evaporation of any reactants such as ethanol, which harmfully obstruct the chemical reactions taking place. In addition, Fathi and Hanifi (2009) proved that the increase of the aging time greater than 36 h leads to the extra removal of the structural water which leads to the decomposition of the HA to TCP and CaO. So, according to these works (Fathi and Hanifi 2009; Tredwin et al. 2009), the increase of the temperature or time leads to removal of the structural water, and as consequence, ß-TCP is formed.

As demonstrated in Table 2, either the crystallinity degree or the crystallite size of HA increases slightly with aging temperature until 70 °C, which confirms the XR results. As presented in Table 2, the values of the Ca/P molar ratio; in all prepared powders; were generally superior to that of the stoichiometric molar ratio in HA or TCP (for 90 °C). This can be justified by the presence of the second phase CaO as shown by XR patterns. Or; the calculated Ca/P molar ratio decreased (from 4.10 to 1.78) with the aging temperature and moved toward the stoichiometric molar ratio in HA for 70 °C (1.97) and mainly for 90 °C (1.78) aging temperature. As mentioned previously, the amount of CaO decreased with aging temperature, which leads, consequently, to the decrease of the Ca/P molar ratio.

Figure 8 shows FTIR of the prepared powders versus the aging temperature. Infrared absorption spectra of 25, 50, and

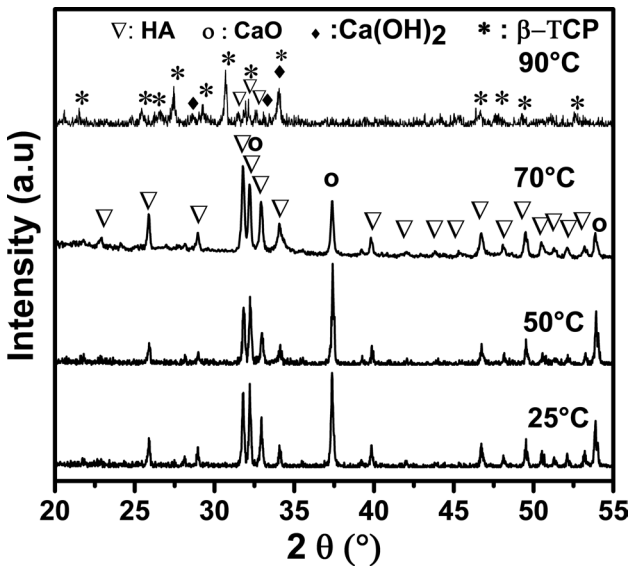

Fig. 7 XRD patterns of prepared powders versus the aging temperature, calcined at 700 °C

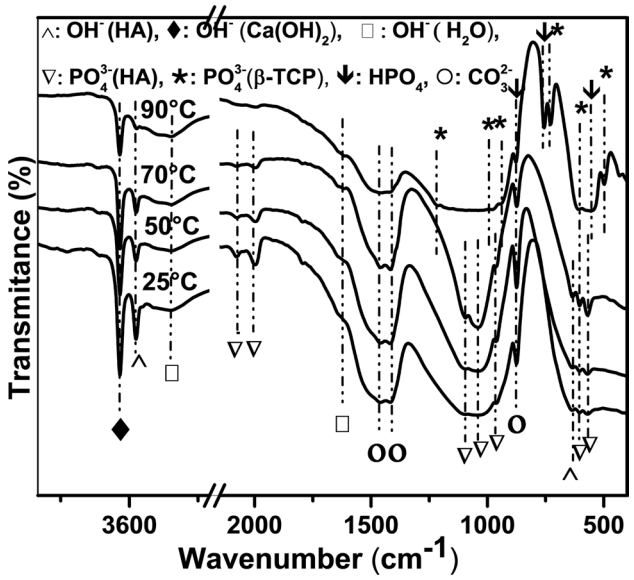

Fig. 8 FTIR spectra of prepared powder versus the aging temperature, calcined at 700 °C

70 °C prove the presence of HA justified by the presence of phosphate groups (PO_4^{3-}) at 568, 604, 959, 1044, and 1093 cm^{-1} and the OH^- groups at 639 and 3573 cm^{-1} (Koutsopoulos 2002; Joris and Amberg 1971). Also, the adsorbed water was revealed by the presence of the two bands at 1634 and around 3400 cm^{-1} (Koutsopoulos 2002). While, the peaks situated at 879, 1414, and 1464 cm^{-1}, indicate the presence of the carbonate groups. As demonstrated, the peak at 879 cm^{-1} can be also assigned to the (HPO_4) group characteristic of deficient HA (Vignoles et al. 1989). It can be observed that the intensity of the characteristic bands of HA increased and became narrower with aging temperature. The observed peak at 3640 cm^{-1} is assigned to the stretching mode of O–H in $Ca(OH)_2$. However, for 90 °C aging time, the intensity of peaks assigned to HA becomes very weak. But the new peaks that appeared at 498, 726, 943, and 985 cm^{-1} are assigned to the β-tricalcium phosphate (β-TCP) phase. Also, the peak at 604 cm-^{1} can be assigned to β-TCP (Jillavenkatesa and Condrate 1998). The bands situated at 546,756, 879, and 1211 cm^{-1} are characteristic of HPO_4 (Gentile et al. 2015). It is clear that the intensity of characteristic bands of HA decreases and also the band centered at 1080 cm^{-1} becomes shoulder, which denotes that a minor deficient HA is formed. FTIR results are in well accordance with XRD analysis.

As presented in Fig. 9, TG-DSC curves exhibit different variations with temperature. For 25 °C, TG curve presents three major changes. Two successive weight losses (24% and 48%) are observed at the intervals 30–200 °C and 200–723 °C. The first weight loss corresponds to the departure of the volatile products resulting from the hydrolysis of TEP, such as ethanol, adsorbed water and structural water resultant from the dehydration of nitrates. This result is confirmed by the apparition of the endothermic peaks at 159 and 190 °C. The second weight loss is remarkable. It corresponds to the pyrolysis process of organic compounds and the decomposition of the calcium nitrate. A large exothermic peak (290–400 °C) with very low intensity was observed. Also, two endothermic peaks appeared around 561 and 721 °C. The first peak presents the melting temperature of calcium nitrate, whereas the second peak corresponds to the liquid solution decomposition into calcium oxide, nitrogen dioxide, and oxygen (Vollmer and Ayers 2012; Yuvaraj et al. 2003). After 723 °C, the weight loss is constant. The exothermic peak at 663 °C corresponds probably to the crystallization temperature of hydroxyapatite. For 70 °C, the TG curve is detailed elsewhere. Otherwise, for 90 °C, the TG curve showed three successive weights losses. A similar weight loss (20%) was observed at the intervals 30–150 °C and 150–256 °C. The first weight loss corresponds to the departure of the volatile products resulting from the hydrolysis of TEP, such as ethanol and adsorbed water. The second weight-loss corresponds to the departure of structural water resultant from the dehydration of nitrates justified by the apparition of the large endothermic peak around 150 °C. However, in the interval 256–272 °C, a fast decrease in weight loss (31%) was noticed. It corresponds to the pyrolysis process of organic compounds justified by the apparition of the narrow exothermic peak at 266 °C. After 272 °C, the mass loss decreases slightly until 600 °C, where it becomes constant. According to XR results, the exothermic peak at 682 °C corresponds probably to the crystallization temperature of β-tricalcium phosphate (β-TCP). It can be observed that the temperature of the pyrolysis process of organic compound decreased with aging temperature and the corresponding peak became narrower and higher. According to Vijayalakshmi and Rajeswari (2012), the decomposition of calcium nitrate gives oxidizing gaseous products and is

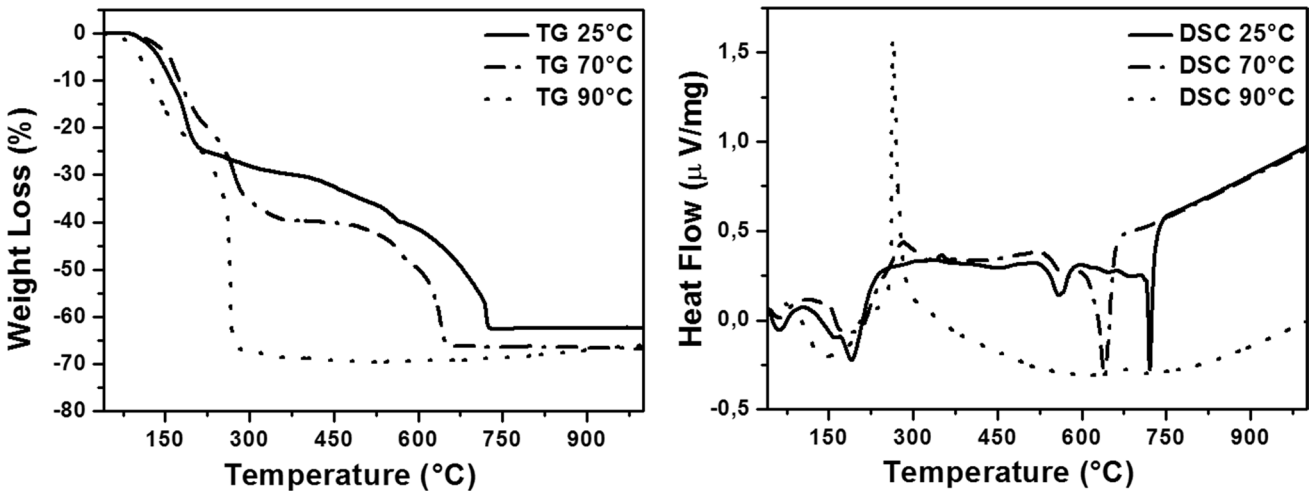

Fig. 9 TG-DSC curves of prepared powders, versus the aging temperature, calcined at 700 °C

very helpful in removing the organic residues at a relatively low temperature. During the reaction of calcium nitrate with TEP, calcium carbonate was formed in addition to HA as a major phase. As previously mentioned, the formation of carbonate groups is due to the presence of ethyl radicals in the dried powder, which arises from the TEP precursor. They have also suggested the departure of NO_2 and CO_2 at 300 °C (Vijayalakshmi and Rajeswari 2012). The comparison of our results with those of Vijayalakshmi and Rajeswari (2012) leads to conclude that the departure of NO_2 occurred during the pyrolysis of organic compounds at around 266 °C. Moreover, the formed $CaCO_3$ continued to decompose until 700 °C.

After 261 °C, the TG curves illustrate that the weight loss of gel aged at 25 °C is less by about 5–10% than that of gel aged at 70 and 90 °C. This difference is the result of more pyrolysis of organic compounds in gels aged at 70 and 90 °C as confirmed by the DSC results.

Figures 10 and 11 present the size distribution and micrographs of powders versus the aging temperature. Generally, all dried gels exhibit a similar morphology and show a mixture between agglomerates and fine particles were observed with a bimodal distribution. For 25 °C, the size distribution of the fine particles fluctuates between 0.17 and 0.7 µm. However, for the other temperatures, it fluctuates between 0.07 and 0.5 µm. Or, the second distribution varies between 0.6 and 30 µm. It can be observed that for 25 °C aging temperature, the powder comprises minor fine particles and tended to agglomerate strongly in comparison to other temperatures. Also, the maximum frequency decreases with aging temperature from 7.7 to 3.4 µm (D_{50} = 5.94 µm, D_{90} = 11.39 µm (25 °C) / D_{50} = 2.62 µm, D_{90} = 5.53 µm (90 °C)). The results of the size distribution are in well accordance with the micrographs. As the aging time increases, the size of the agglomerates decreases and also their shape becomes more homogeneous (spherical shape). Certainly the decrease in grain size leads to the further agglomeration of particles and consequently, the increase in agglomerates size. As a result, for 90 °C aging temperatures, the particles mainly attributed to β-TCP are very fine in comparison to other aging temperatures.

As the temperature increases, the hydrolysis of TEP is improved and consequently, the condensation of the resulted products with the calcium ions dissolved in the solution during aging. So, either the increase in temperature or time leads to formation of further (-Ca-O-P-) bonds in the dry gels (Beganskienė et al. 2003). As a consequence, the cross-linked structure of the molecules increases and favors the

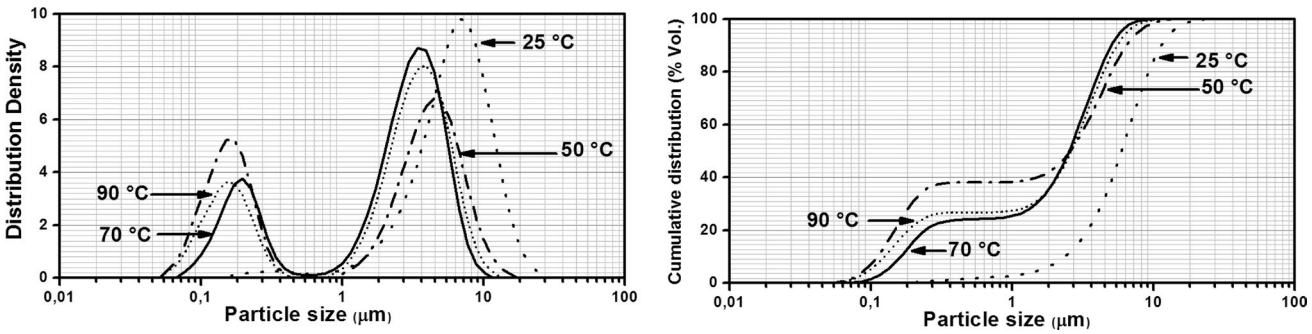

Fig. 10 Particle size distribution of prepared powders, versus the aging temperature, calcined at 700 °C

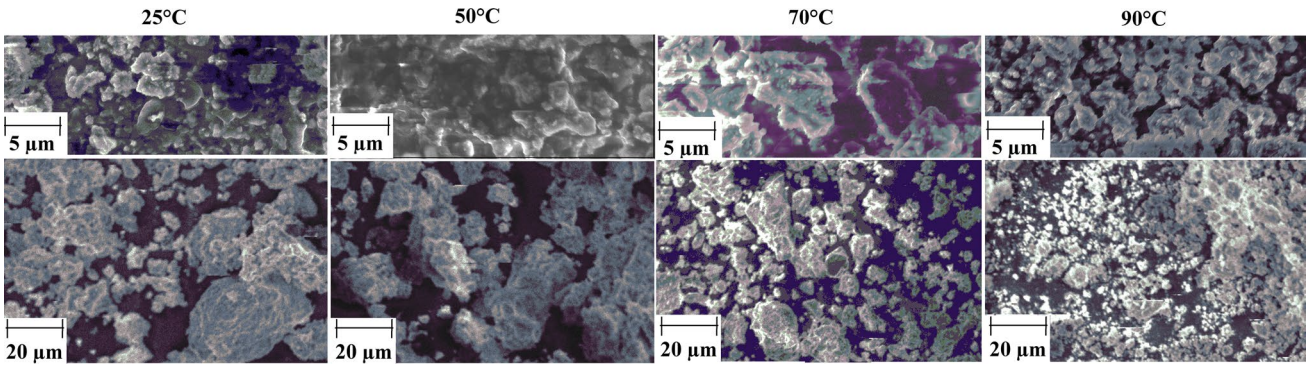

Fig. 11 SEM micrographs of prepared powders, versus the aging temperature, calcined at 700 °C

formation of large crystallite of well-crystallized HA (Fathi and Hanifi 2009; Balamurugan et al. 2006; Santos et al. 2015). But, the aging temperature must not exceed 70 °C in order to preserve the structural water and to avoid the β-TCP formation.

Effect of solvents on HA synthesis

Two types of solvent were tested: distilled water and ethanol; the assays were realized as follows:

- Triethyl phosphate was dissolved in distilled water and calcium nitrate was dissolved in ethanol.
- Triethyl phosphate was dissolved in ethanol and distilled water and calcium nitrate was dissolved in ethanol.
- Triethyl phosphate was dissolved in ethanol and distilled water and calcium nitrate was dissolved in distilled water.
- Triethyl phosphate and calcium nitrate were dissolved in distilled water.

For all the assays, the obtained solutions were aged at 70 °C for 1 day. The same conditions were chosen for gelling and drying.

pH was identified around 5 as the initial pH for all the obtained solutions at the end of stirring. The pH values were declined to around the zero value after 1 day of aging time at 70 °C. For all assays, TEP was hydrolyzed in the presence of an amount of distilled water in order to increase its reactivity and so that it can react easily with the calcium nitrate. When ethanol is used as a medium solvent, some of the nitrate groups will be replaced and alkyl groups such as $Ca(OR)_y(NO_3)_{2-y}$ will be formed (Balamurugan et al. 2006). Through the aging time, the hydrolyzed phosphorus sol, generally in the form of $PO(OEt)_{3-x}(OH)x$, interacts with Ca sol, probably in the form of $Ca(OEt)_{3-x}(NO_3)_{2-y}$ in anhydrous ethanol and Ca^{2+} in water, to form oligomeric derivatives containing Ca-O-P bonds. According to the hydrolysis reaction of triethyl phosphite described by Liu et al. (2001), the ethanol-based process of triethyl phosphate may proceed as follows:

$$\begin{aligned}&\mathbf{PO(OEt)_{3-x}(OH)_x + Ca\left(NO_3\right)_{2-y}(OEt)_y}\\&\quad\rightarrow \mathbf{(OEt)_{y'}\left(NO_3\right)_{2-y'} - Ca - O - HPO(OEt)_{3-x'}}\\&\qquad\mathbf{+ H_2O + C_2H_5OH}\end{aligned} \tag{6}$$

For the distilled water-based process, the reaction was described earlier (Eq. 3).

Figure 12 shows X-ray patterns for prepared samples versus the used solvents. Generally, XRD patterns reveal the same existent phases (HA and CaO) for all cases. However, just for the two cases (Ca + DW/TEP + DW and Ca + DW/TEP + DW + Eth), the intensity of peaks characteristic of HA is higher than that of CaO. In addition, in the case of (Ca + DW/TEP + DW), the HA peaks are more narrow and better in comparison to all cases. It can be observed that the decrease of the amount of water leads to a decrease in the intensity of peaks characteristic of HA and also the peaks are sharp in comparison when 30 mL of distilled water is used to prepare HA. Kim et al. (2004) showed that the use of the reduced amount of water than 30 mL did not lead to the sol-gel production. As a consequence, TEP was not sufficiently reactive when mixed with calcium nitrate and HA sol–gel was not produced. In the process of hydrolysis, the electrons from the water attack the phosphate in the TEP and cause the terminal group with organically bound oxygen to be displaced and replaced by an –OH group. So, an inadequate amount of water leads to insufficient electrons to attack the phosphate groups in the TEP. So, the distilled water with an adequate amount is necessary for TEP hydrolysis.

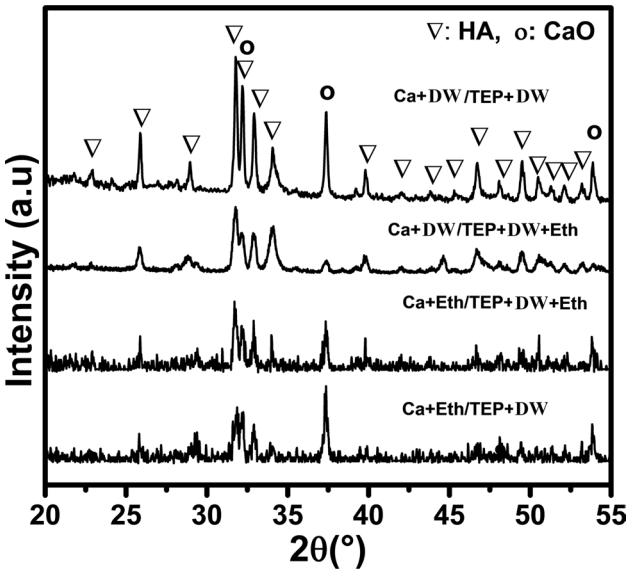

Fig. 12 XRD patterns of prepared powders and versus the medium solvent, calcined at 700 °C

Table 3 Crystallite size, crystallinity, and molar ratio (Ca/P) for the prepared powders versus the medium solvent

Sample	Crystallite size (nm)	Crystallinity (%)	Molar ratio Ca/P
Ca + Eth/TEP + DW	20.45	69	3.03
Ca + Eth/TEP + Eth + DW	21.97	79	2.99
Ca + DW/TEP + Eth + DW	55.32	91	2.67
Ca + DW/TEP + DW	58.54	93	1.97

As demonstrated in Table 3, either the crystallinity degree or the crystallite size increases considerably with the amount of distilled water, which confirms the XR results.

Furthermore, the value of the Ca/P molar ratio (Table 3); in all prepared powders; was superior to that of the stoichiometric molar ratio in HA. This can be justified by the presence of the second phase CaO as shown by XR patterns. Or; the calculated Ca/P molar ratio decreased (from 3.03 to 1.97) with the increase of the amount of the distilled water and moved toward the stoichiometric molar ratio in HA when using only the distilled water as solvent. As mentioned previously, the amount of CaO decreased with the increase of the amount of distilled water, which led consequently to the decrease of the Ca/P molar ratio.

Figure 13 compares the FTIR spectra of the HA prepared and calcined powders at 700 °C versus the solvent: distilled water and ethanol. In Fourier-transform infrared spectroscopy, the domain from 500 to 700 cm^{-1} is used to describe the apatite structure. The obtained results confirm the presence of the phosphate (PO_4^{3-}) (Koutsopoulos 2002; Joris and Amberg 1971) and the hydroxyl (Hosseini et al. 2017) groups in all spectra, as previously described. But there is a difference in their intensity and the broadness of these peaks. They become narrower and their intensities increase with the amount of used water. Also, the two peaks at 1414 and 1464 cm^{-1} indicate the presence of the carbonate group (Vignoles et al. 1989). It should be noted that the absorption peak at 879 cm^{-1} can be due to the carbonate group or to the (HPO_4) group characteristic of deficient HA. The observed peak at 3640 cm^{-1}, characteristic of OH^- mode, confirms the presence of Ca $(OH)_2$, in all the prepared powders. FTIR results confirm the XRD analysis.

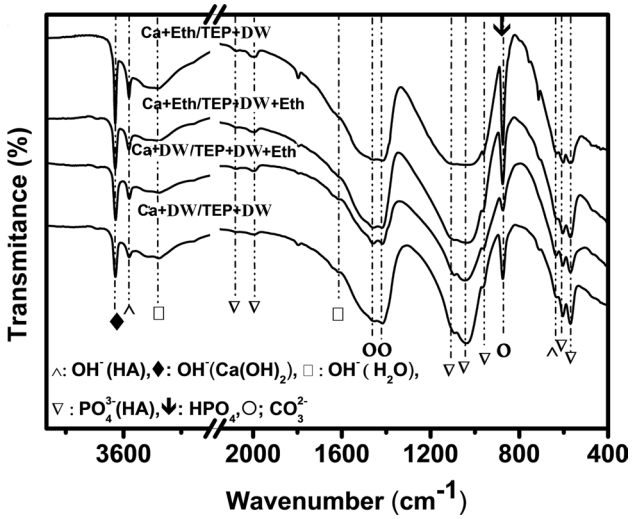

Fig. 13 FTIR spectra of prepared powders versus the medium solvent, calcined at 700 °C

All the TG-DSC curves as a function of solvent exhibit generally the same trend (Fig. 14). The curves showed approximately four identical weight loss stages such as: 30–150 °C, 150–350 °C, 50–500 °C, and 500–650 °C. No further weight loss was renowned from 650 °C. The first weak weight-loss corresponds to the departure of the volatile products resulting from the hydrolysis of TEP, such as ethanol and adsorbed water. In the second broad loss, the weight loss is remarkable. It corresponds to the departure of structural water resulting from the dehydration of nitrates and the pyrolysis process of organic compounds. The presence of two exothermic peaks for the solvent 25% Eth + 5% DW can be observed. Perhaps there are different organic compounds resulting from the difference of the used solvent. At the third stage, the weight loss is very low. Also in the fourth stage, the weight loss is significant where different endothermic peaks appeared. The first peak is around 572 °C for all different solvents; it presents the melting temperature of calcium nitrate. Or, the other endothermic peaks were

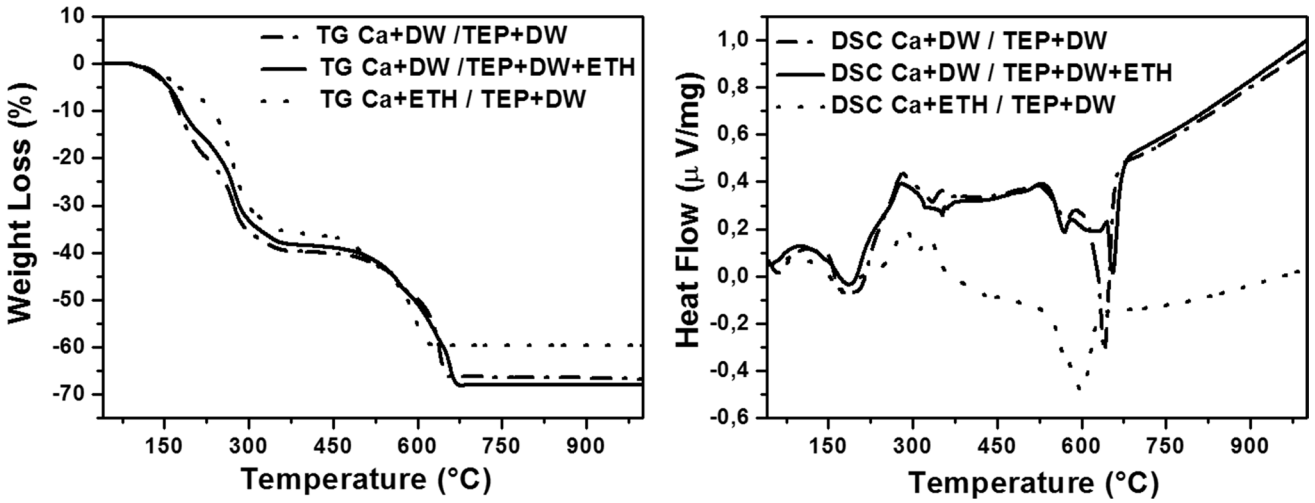

Fig. 14 TG-DSC curves of prepared powders, versus the medium solvent, calcined at 700 °C

appeared around 600 or/and 640 °C, they correspond to the liquid solution decomposition of calcium nitrate (Vollmer and Ayers 2012; Yuvaraj et al. 2003). It can be observed that the decomposition temperature of calcium nitrates is different from the type of solvent. According to Liu et al. (2001), in anhydrous ethanol, the nitrate groups can be replaced by the alkyl groups which leads to the formation of the alkoxynitrate species in the dry gel Ca(OR)*y*(NO3)2-y. In addition, the decomposition temperature of calcium nitrates mentioned in literature is different from a work to another, for example: 285 °C (Liu et al. 2002), 340 °C (Anjaneyulu et al. 2016), 364 °C (Vijayalakshmi and Rajeswari 2012), 400 °C (Fathi and Hanifi 2009), 300–520 °C (Liu et al. 2001) and 602 °C (Yuvaraj et al. 2003). So, the mixture of ethanol and distilled water, with different ratios, led to the formation of different alkoxynitrate species in Ca(OR)*y*(NO3)2-y and consequently, different decomposition temperatures. Moreover, the obtained results show that the weight loss ratio decreases from 66 to 60% when the amount of ethanol present in the solvent decreases from 25 to 5 mL (or also without ethanol). The difference in weight loss started at the first stage. Perhaps the HA prepared in distilled water contains a greater amount of residual water resultant from complete hydrolysis of TEP and subsequently more formation of P–O–Ca than in other solvents. Noted that Liu et al. (2001) have demonstrated that weight loss in the HA prepared in ethanol as solvent is less 2 wt.% than prepared in distilled water. Certainly, the difference in the used phosphorus precursors (triethyl phosphite and the drying temperature of gel at 60 °C (Liu et al. 2001) led to the difference in the results of the two works.

It can be remarked that in our entire work, the sample characterized by more crystallized HA is the sample with the high weight loss ratio. So, this confirms our suggestion that the greater amount of residual water is present in gel in which the complete hydrolysis of TEP and subsequently the more formation of P–O–Ca were occurred.

Figures 15 and 16 present the size distribution and micrographs of powders as a function of amount of the distilled water. Generally, all dried gels exhibit a similar morphology and show a mixture between agglomerates and fine particles were observed with a bimodal distribution. Generally, the size distribution of the fine particles fluctuates between 0.07 and 0.5 µm. Or, the second distribution varies between 0.6 and 25 µm. It can be observed that just for the distilled water, the powder comprises remarkable fine particles and tended to agglomerate softly in comparison to other solvent mediums. Also, the maximum frequency decreases with

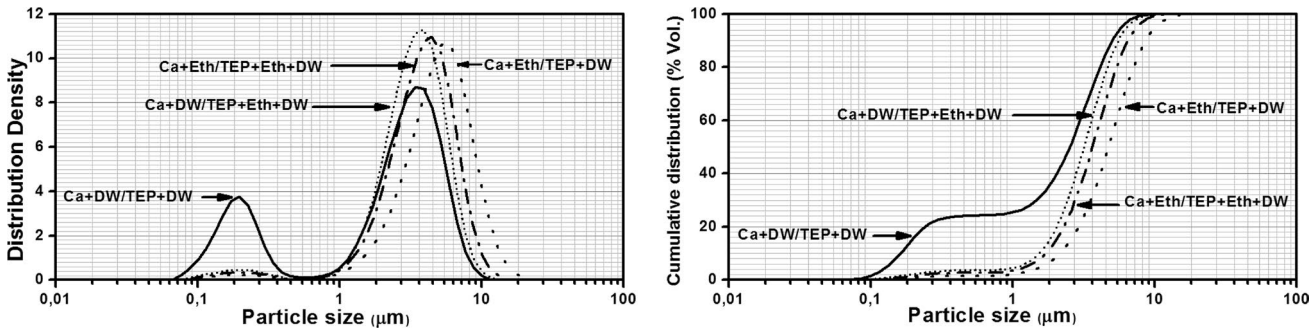

Fig. 15 Particle size distribution of prepared powders, versus the medium solvent, calcined at 700 °C

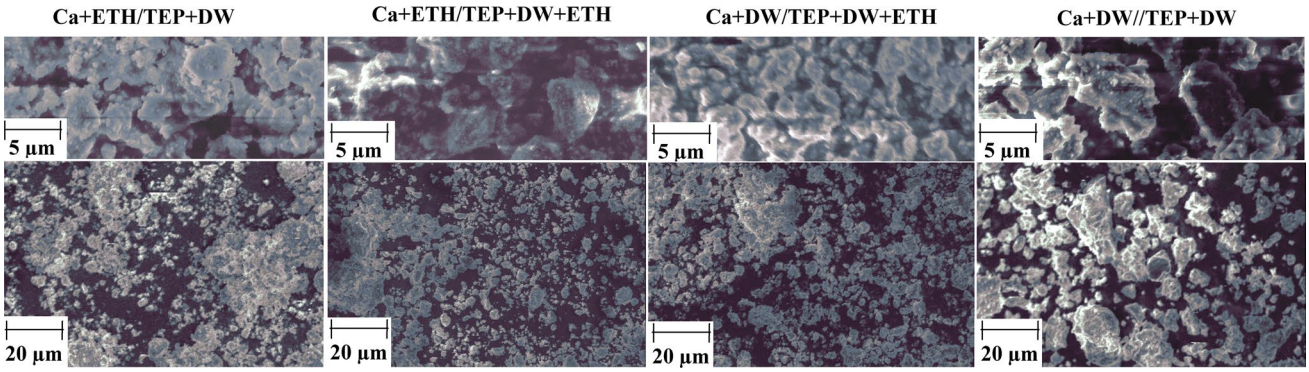

Fig. 16 SEM micrographs of prepared powders, versus the medium solvent, calcined at 700 °C

increase of the amount of the distilled water from 5.9 to 3.4 µm (D_{50} = 4.74 µm, D_{90} = 8.63 µm (V(DW) = 5 mL)/ D_{50} = 2.52 µm, D_{90} = 5 µm (V(DW) = 30 mL)). The results of the size distribution are in well accordance with the micrographs. As the amount of the distilled water increases, the size of the agglomerates decreases and also they become more distinguishable. As mentioned previously, the decrease of grain size leads to the further agglomeration of particles and consequently the increase of agglomerates size.

According to the obtained results, as the amount of distilled water increases, the hydrolysis of TEP is improved, and consequently, the condensation of the resulted products with the calcium ions dissolved in the solution during aging. So, further (-Ca-O-P-) bonds in the dry gels are formed (Beganskienė et al. 2003). Hence, the cross-linked structure of the molecules increases and favors the formation of large crystallite of well-crystallized HA (Fathi and Hanifi 2009; Balamurugan et al. 2006; Santos et al. 2015).

The comparison of our findings to that of other researchers (Hsieh et al. 2001; Chandanshive et al. 2013; Vijayalakshmi and Rajeswari 2006) reveals that aging of mixed precursors in closed Teflon® container has a positive effect. The reactivity and the hydrolysis of TEP were optimized. Accordingly, the hydrolyzed phosphorus sol interacted with the Ca sol, in the form of Ca^{2+} ions in water, to form oligomeric derivatives containing Ca-O-P bonds during the aging process in a closed Teflon® container. So, the optimization of the hydrolysis and the polymerization of TEP at the same time led to reducing the phosphorus volatilization (Fathi et al. 2008) during the gelling process which was done in an opened container. The values of Ca/P molar ratio and the amount of CaO present in prepared powders confirmed this suggestion. The values of Ca/P molar ratio decreased and approached stoichiometric value in HA when the hydrolysis and polymerization of TEP were optimized. Also, the amount of CaO decreased. Consequently, the aging time and temperature were strongly decreased. Hsieh et al. synthesized HA by sol–gel route using the calcium nitrate tetrahydrate and triethyl phosphate. The prepared sols were put in, tightly capped and dried in an oil bath at 80 and 90 °C for 48 h. After that, the dried gels were calcined up to 600 °C. XRD patterns revealed major peaks of hydroxyapatite and a weak CaO peak (Hsieh et al. 2001). Also, Chandanshive et al. (2013) used the triethyl phosphate and calcium nitrate tetrahydrate for HA synthesis by sol–gel route. The sols were aged at 80 °C for 48 h. XRD of calcined gel at 900 °C revealed the formation of the crystalline HA phase as major phase and a minor phases: CaO and β-TCP. Furthermore, Vijayalakshmi and Rajeswari (2006) explored triethyl phosphate for HA synthesis. But, they used the calcium acetate as calcium precursor. The sols were prepared in a nitrogen atmosphere glove box. The solution was aged for 24 h. Then, the formed gels were dried at 120 °C for 16 h. They used two different medium solvents: distilled water and ethanol. XRD patterns of the sample heated at 900 °C showed the presence of a major apatite phase and a second phase of calcium carbonate (Vijayalakshmi and Rajeswari 2006). In all these works, they used either longer aging time and temperature higher than 70 °C or a specific atmosphere. However, in the present work, a well-crystallized HA was obtained by using simple conditions of synthesis (closed Teflon container®) and in short time and lower temperature than in other research. Moveover HA crystallization occurred at low temperature (≈ 350 °C) as reported in the work of Liu et al. (2001). This value is very low in comparison to other works (Gross et al. 1998a; b; Balamurugan et al. 2006; Beganskienė et al. 2003). In view of Gross et al. (1998b), an important amount of hydroxyl species (primarily from initial water addition) present within the gel may possibly be responsible for the low-temperature crystallization.

Many works studied the thermal stability of HA. Tas (2000) reported that HA remained stable until 1300 °C. Also, Vijayalakshmi and Rajeswari (2012) found that HA was stable until 1200 °C. Other researchers established that the stoichiometric HA remained stable below 1200 °C (Fathi and Hanifi 2009; Anjaneyulu et al. 2016; De Groot et al. 1990). For example, Fathi and Hanifi (2009) demonstrated that HA decomposed into tri-calcium phosphate at 700 °C. Elsewhere, Anjaneyulu et al. (2016) recognized that HA decomposed into β-TCP at 900 °C. So, in order to evaluate the thermal stability of HA aged and dried at 70 °C for 24 h, the prepared powder was heated at 1100, 1200, and 1300 °C. XRD results confirmed the HA stability (Fig. 17). The HA decomposition into tri-calcium phosphate or other secondary phase did not occur. Moreover, the XRD patterns illustrated

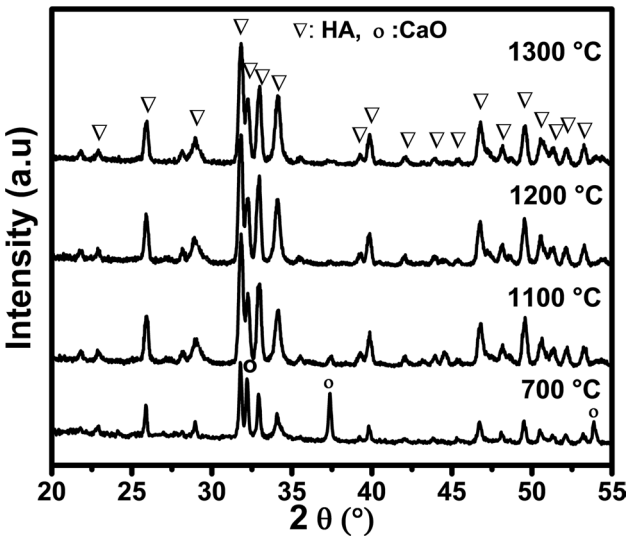

Fig. 17 XRD patterns of HA powder, aged at 70 °C for 1 day, versus the heat treatment temperature

that the amount of CaO decreased with temperature of heat treatment. This result allows suggesting that Ca continued to diffuse into HA structure in order to form well0crystallized HA. So, the hydrolysis of TEP into a closed Teflon container®, prevented its evaporation, performed its reactivity and consequently, optimized the P-O-Ca linkage. As a consequence, the well-crystallized HA was obtained by sol–gel route without decomposition at high temperatures.

Conclusion

In this study, several experiments were undertaken to determine the optimal conditions for the preparation of well-crystallized hydroxyapatite by using the sol–gel route. Triethyl phosphate and calcium nitrate were used as phosphorus and calcium precursors, respectively. In order to optimize the hydrolysis of TEP, the aging of sols was carried in a closed Teflon container®. So, this study detailed the effect of aging time (4, 16 and 24 h), aging temperature (25, 50, 70, and 90 °C), and solvents (distilled water and/or ethanol) on the synthesis of hydroxyapatite. All prepared powders were calcined at 700 °C. The results, obtained by X-ray diffraction and infrared spectrometry, confirmed the formation of the crystalline hydroxyapatite in all cases. The intensity of HA peaks increased with aging time and temperature, which must not exceed 70 °C. When the temperature exceeded 70 °C, the tri-calcium phosphate as a major phase and hydroxyapatite as a minor phase was formed. However, for the type of solvent, this study demonstrated that the presence of the appropriate amount of water is important for the hydrolysis of TEP and also for the well-crystallization of HA. The optimal conditions of HA preparation by sol–gel route are 24 h as aging time and 70 °C as aging temperature. In addition, the degree of HA crystallization was the best under these conditions. It can be remarked that the aging of sols in a closed Teflon container® leads to an important decrease of the aging time and temperature in comparison to other studies. In addition, a well-crystallized hydroxyapatite was formed without any decomposition at high temperatures.

Acknowledgments Many thanks to Boubakeur Saidat, Bachir Helifa, Omar Allaoui (Laboratoire physico-chimie des matériaux LPCM, Université Amar Telidji- Laghouat), Abdelfetteh Sayah and Abdelghani Rahal (Research Unit on Emerging Materials (RUEM), Ferhat Abbas University- Setif) for their fruitful collaborations.

Declarations

Conflict of interest The authors declare that they have no conflict of interest.

References

Andrasekhar A, Sagadevan S, Dakshnamoorthy A (2013) Synthesis and characterisation of nano- hydroxyapatite (n-HAP) using the wet chemical technique. Int J Phys Sci 8:1639–1645

Anjaneyulu U, Pattanayak DK, Vijayalakshmi U (2016) Snail shell derived natural hydroxyapatite: effects on NIH-3T3 cells for orthopedic applications. Mater Manuf Proc 31(2):206–216. https://doi.org/10.1080/10426914.2015.1070415

Bakan F, Laçin O, Sarac H (2013) A novel low temperature sol–gel synthesis process for thermally stable nano crystalline hydroxyapatite. Powder Technol 233:295–302. https://doi.org/10.1016/j.powtec.2012.08.030

Balamurugan A, Michel J, Faure J, Benhayoune H, Wortham L, Sockalingum G, Banchet V, Bouthors S, Laurent-Maquin D, Balossier G (2006) Synthesis and structural analysis of sol gel derived stoichiometric monophasic hydroxyapatite. Ceram Silikáty 50:27–31

Beganskienė A, Dudko O, Sirutkaitis R, Giraitis R (2003) Water based sol-gel synthesis of hydroxyapatite. Mater Sci 9(4):383–386

Ben-Nissan B, Green DD, Kannangara GSK, Chai CS, Milev A (2001) 31P NMR studies of diethyl phosphite derived nanocrystalline hydroxyapatite. J Sol-Gel Sci Technol 21:27–37. https://doi.org/10.1023/A:1011281826850

Bilton M, Brown AP, Milne SJ (2010) Sol-gel synthesis and characterisation of nano-scale hydroxyapatite. J Phy Conf Ser 241:012052. https://doi.org/10.1088/1742-6596/241/1/012052

Chandanshive BB, Rai P, Rossi AL, Ersen O, Khushalani D (2013) Synthesis of hydroxyapatite nanotubes for biomedical applications. Mater Sci Eng C 33:2981–2986. https://doi.org/10.1016/j.msec.2013.03.022

Chen J, Wang Y, Chen X, Ren L, Lai C, He W, Zhang Q (2011) A simple sol–gel technique for synthesis of nanostructured hydroxyapatite, tricalcium phosphate and biphasic powders. Mater Lett 65:1923–1926

Chung RJ, Hsieh MF, Huang KC, Perng LH, Chou FI, Chin TS (2005) Anti-microbial hydroxyapatite particles synthesized by a sol-gel route. J Sol-Gel Sci Techno 33:1–11. https://doi.org/10.1007/s10971-005-5618-1

Cihlar J, Castkova K (1984) Synthesis of calcium phosphates from alkyl phosphates by the sol–gel method. Ceram Silikáty 2:164–170

de Groot K, Klein CPAT, Wolke JGC, de Bliek-Hogervost JMA (1990) Chemistry of Calcium Phosphate Bioceramics. In: Yamamuro T, Hench LL, Wilson J (eds) Handbook of Bioactive Ceramics, vol 2. CRC Press, Boca Raton, Florida, pp 3–16

Dinu E, Birsan M, Ghitulica C, Voicu G, Andronescu E (2013) Synthesis and characterization of hydroxyapatite obtained by sol–gel method. Roman J Mater 43:55–60

dos Santos ML, Riccardi CS, Noronha AL, de Olyveira GM, Filho EA, Guastaldi AC (2015) Effect of aging time on calcium phosphates powders obtained by sol-gel method. Mater Sci Indian J 12(12):444–448

Eshtiagh-Hosseini H, Housaindokht MR, Chahkandi M (2007) Effects of parameters of sol–gel process on the phase evolution of sol–gel-derived hydroxyapatite. Mater Chem Phys 106:310–316

Fathi MH, Hanifi A (2009) Sol–gel derived nanostructure hydroxyapatite powder and coating: aging time optimization. Adv Appl Ceram 108:363–368. https://doi.org/10.1179/174367609X414080

Fathi MH, Hanifi A, Mortazavi V (2008) Preparation and bioactivity evaluation of bone-like hydroxyapatite nanopowder. J Mater Process Tech 202:536–542. https://doi.org/10.1016/j.jmatprotec.2007.10.004

Ferraz MP, Monteiro FJ, Manual CM (2004) Hydroxyapatite nanoparticles: a review of preparation methodologies. J App Biomater Biomech 2:74–80

Gentile P, Wilcock CJ, Miller CA, Moorehead R, Hatton PV (2015) Process optimisation to control the physico-chemical characteristics of biomimetic nanoscale hydroxyapatites prepared using wet chemical precipitation. Materials 8(5):2297–2310. https://doi.org/10.3390/ma8052297

Ghosh SK, Roy SK, Kundu B, Datta S, Basu D (2011) Synthesis of nano-sized hydroxyapatite powders through solution combustion route under different reaction conditions. Mater Sci Eng B 176:14–21. https://doi.org/10.1016/j.mseb.2010.08.006

Glimsher MJ (1984) Recent studies of the mineral phase in bone and its possible linkage to organic matrix by protein-bound phosphate bonds. Philos Trans R Soc Lond B Biol Sci 304:479–508. https://doi.org/10.1098/rstb.1984.0041

Green DD, Kannangara GSK, Milev A, Ben-Nissan B (1999) Characterisation of a new alkoxide sol-gel hydroxyapatite. In: proceedings 11 Australian Conference on nuclear techniques of analysis and the 5th vacuum society of Australia congress, pp. 186–188

Gross KA, Gross V, Berndt CC (1998a) Thermal analysis of amorphous phases in hydroxyapatite coatings. J Am Ceram Soc 81(1):106–112. https://doi.org/10.1111/j.1151-2916.1998.tb02301.x

Gross KA, Chai CS, Kannangara GSK, Ben-Nissan B, Hanley L (1998b) Thin hydroxyapatite coatings via sol–gel synthesis. J Mater Sci Mater Med 9:839–843. https://doi.org/10.1023/A:1008948228880

Hosseini B, Mirhadi SM, Mehrazin M, Yazdanian M, Motamedi MRK (2017) Synthesis of nanocrystalline hydroxyapatite using eggshell and trimethyl phosphate

Hsieh MF, Perng LH, Chin TS, Perng HG (2001) Phase purity of sol gel-derived hydroxyapatite ceramic. Biomaterials 22:2601–2607. https://doi.org/10.1016/s0142-9612(00)00448-8

Ioitescu A, Vlase G, Vlase T, Ilia G, Doca N (2009) Synthesis and characterization of hydroxyapatite obtained from different organic precursors by sol–gel method. J Therm Anal Calorim 96:937–942. https://doi.org/10.1007/s10973-009-0044-1

Ishikawa K, Kareiva A (2020) Sol–gel synthesis of calcium phosphate-based coatings– a review. Chemija 31(1):25–41. https://doi.org/10.6001/chemija.v31i1.4169

Ishikawa K, Garskaite E, Kareiva A (2020) Sol–gel synthesis of calcium phosphate-based biomaterials—a review of environmentally benign, simple, and effective synthesis routes. J Sol-Gel Sci Techno. https://doi.org/10.1007/s10971-020-05245-8

Jenkins R, Snyder RL (1996) Introduction to X-ray powder diffractometry. John Wiley & Sons, New York

Ji X, Su P, Liu C, Song J, Li J, Tan H, Wu F, Yang L, Fu R, Tang C, Cheng B (2015) A novel ethanol induced and stabilized hierarchical nanorods: hydroxyapatite nanopeanut. J Am Ceram Soc 98:1702–1705

Jillavenkatesa A, Condrate RA (1998) The infrared and raman spectra of β-and α-tricalcium phosphate ($Ca_3(PO_4)_2$). Spectrosc Lett 31(8):1619–1634. https://doi.org/10.1080/00387019808007439

Johnson DW (1985) Sol-gel processing of ceramics and glass. Amer Ceram Soc Bull 64:1597–1604

Jonauskė V, Stanionyte S, Chen SW, Zarkov A, Juskenas R, Selskis A, Matijosius T, Yang TCK, Ishikawa K, Ramanauskas R, Kareiva A (2019) Characterization of sol-gel derived calcium hydroxyapatite coatings fabricated on patterned rough stainless steel surface. Coatings 9(5):334

Joris SJ, Amberg CH (1971) Nature of deficiency in nonstoichiometric hydroxyapatites. II. Spectroscopic studies of calcium and strontium hydroxyapatites. J Phys Chem 75:3172–3178. https://doi.org/10.1021/j100689a025

Joschek S, Nies B, Krotz R, Göpferich A (2000) Chemical and physicochemical characterization of porous hydroxyapatite ceramics made of natural bone. Biomaterials 21:1645–1658. https://doi.org/10.1016/s0142-9612(00)00036-3

Kalita SJ, Bhatt HA (2007) Nanocrystalline hydroxyapatite doped with magnesium and zinc: synthesis and characterization. Mater Sci Eng C 27:837–848. https://doi.org/10.1016/j.msec.2006.09.036

Kalita SJ, Bhardwaj A, Bhatt HA (2007) Nanocrystalline calcium phosphate ceramics in biomedical engineering. Mater Sci Eng C 27:441–449. https://doi.org/10.1016/j.msec.2006.05.018

Kamalanathan P, Ramesh S, Bang LT, Niakan A, Tan CY, Purbolaksono J, Chandran H, Teng WD (2014) Synthesis and sintering of hydroxyapatite derived from eggshells as a calcium precursor. Ceram Int 40:16349–16359. https://doi.org/10.1016/j.ceramint.2014.07.074

Kheimehsari H, Izman S, Shirdar MR (2015) Effects of HA-coating on the surface morphology and corrosion behavior of a co-cr-based implant in different conditions. J Mater Eng Perform 24:2294–2302

Kim HW, Long-Hao L, Koh TH, Knowles JC, Kim HE (2004) Sol-gel preparation and properties of fluoride-substituted hydroxyapatite powders. J Am Ceram Soc 87:1939–1944. https://doi.org/10.1111/j.1151-2916.2004.tb06344.x

Kongsri S, Janpradit K, Buapa K, Techawongstien S, Chanthai S (2013) Nanocrystalline hydroxyapatite from fish scale waste: preparation, characterization and application for selenium adsorption in aqueous solution. Chem Eng J 215–216:522–532. https://doi.org/10.1016/j.cej.2012.11.054

Kordas G, Trapalis CC (1997) Fourier transform and multi dimensional EPR spectroscopy for the characterization of hydroxyapatite gels. J Sol-Gel Sci Technol 9:305–309. https://doi.org/10.1007/BF02436856

Koutsopoulos S (2002) Synthesis and characterization of hydroxyapatite crystals: a review study on the analytical methods. J Biomed Mater Res 62:600–612. https://doi.org/10.1002/jbm.10280

Liu DM, Troczynski T, Tseng WJ (2001) Water-based sol–gel synthesis of hydroxyapatite: process development. Biomaterials 22:1721–1730. https://doi.org/10.1016/s0142-9612(00)00332-x

Liu DM, Yang Q, Troczynski T, Tseng WJ (2002) Structural evolution of sol–gel-derived hydroxyapatite. Biomaterials 23:1679–1687. https://doi.org/10.1016/s0142-9612(01)00295-2

Malakauskaitė-Petruleviciene M, Stankeviciūtė Z, Niaura G, Garskaite E, Beganskiene A, Kareiva A (2016) Characterization of sol-gel processing of calcium phosphate thin films on silicon substrate by FTIR spectroscopy. Vibr Spectrosc 85:16–21. https://doi.org/10.1016/j.vibspec.2016.03.023

Masuda Y, Matubara K, Sakka S (1990) Synthesis of hydroxyapatite from metal alkoxides through sol–gel technique. J Ceram Soc Jpn 98:1255–1266

Mezahi F, Harabi A, Zouai S, Achour S, Bernache-Assollant D (2005) Effect of stabilised ZrO_2, Al_2O_3 and TiO_2 on sintering of hydroxyapatite. Mater Sci Forum 492–493:241–248

Mezahi FZ, Oudadesse H, Harabi A, Lucas-Girot A, Le Gal Y, Chaair H, Cathelineau G (2009) Dissolution kinetic and structural behaviour of natural hydroxyapatite vs. thermal treatment. J Thermal Anal Calor 95(1):21–29

Mojahedian M, Fahimipour F, Larsen KL, Kalantar M, Bastami F, Omatali N (2016) Ethanol-based sol–gel synthesis of nanocrystalline hydroxyapatite with different calcium phosphorus ratios (ca/p). J Ceram Process Res 17:1138–1142

Negrila CC, Predoi MV, Iconaru SL, Predoi D (2018) Development of zinc-doped hydroxyapatite by sol–gel method for medical applications. Molecules. https://doi.org/10.3390/molecules23112986

Padmanabhan SK, Balakrishnan A, Chu MC, Lee YJ, Kim TN, Cho SJ (2009) Sol–gel synthesis and characterization of hydroxyapatite nanorods. Particuology 7:466–470

Pang YX, Bao X (2003) Influence of temperature, ripening time and calcination on the morphology and crystallinity of hydroxyapatite

nanoparticles. J Eur Ceram Soc 23(10):1697–1704. https://doi.org/10.1016/S0955-2219(02)00413-2
Priyadarshini B, Vijayalakshmi U (2018) Development of cerium and silicon co-doped hydroxyapatite nanopowder and its in vitro biological studies for bone regeneration applications. Adv Powder Technol 29:2792–2803. https://doi.org/10.1016/j.apt.2018.07.028
Qiu Q, Vincent P, Lowenberg B, Sayer M, Davies JE (1993) Bone growth on sol-gel calcium phosphate thin films in vitro. Cells Mater 3(4):351–360
Rhee SH (2002) Synthesis of hydroxyapatite via mechano-chemical treatment. Biomaterials 23:1147–1152. https://doi.org/10.1016/s0142-9612(01)00229-0
Saranya K, Kowshik M, Ramanan SR (2011) Synthesis of hydroxyapatite nanopowders by sol-gel emulsion technique. Bull Mater Sci 34:1749–1753. https://doi.org/10.1007/s12034-011-0386-8
Shalini B, Kumar AR (2019) A Comparative study of hydroxyapatite ($Ca_{10}(PO_4)_6(OH)_2$) using sol–gel and co-precipitation methods for biomedical applications. J Ind Chem Soc 96:25–28
Shi Z, Huang X, Cai Y, Tang R, Yang D (2009) Size effect of hydroxyapatite nanoparticles on proliferation and apoptosis of osteoblast-like cells. Acta Biomaterial 5:338–345. https://doi.org/10.1016/j.actbio.2008.07.023
Song YJ, Wen SL, Li MS, Su QC, Jiang QH (2002) Preparation and physicochemical process of nanosized hydroxyapatite powders with high purity. J Inorg Mater 17:985–991
Stankeviciūtė Z, Malakauskaitė-Petruleviciene M, Beganskienė A, Kareiva A (2013) Sol-gel synthesis of calcium phosphate coatings on Ti substrate using dip-coating technique. Chemija 24(4):288–295
Suchanek W, Yoshimura M (1998) Processing and properties of hydroxyapatite-based biomaterials for use as hard tissue replacement implant. Mater Res 13:94–117. https://doi.org/10.1557/JMR.1998.0015
Tas AC (2000) Combustion synthesis of calcium phosphate bioceramic powders. J Eur Ceram Soc 20:2389–2394
Tredwin CJ (2009) Sol-gel derived hydroxyapatite, fluorhydroxyapatite and fluorapatite coatings for titanium implants. Dissertation, University College London
Vignoles M, Bonel G, Holcomb DW, Young RA (1989) influence of preparation conditions on the composition of type B carbonated hydroxyapatite and on the localization of the carbonate ions. Calcif Tissue Int 45:157–164
Vijayalakshmi U, Rajeswari S (2006) Preparation and characterization of microcrystalline hydroxyapatite using sol gel method. Trends Biomater Artif Organs 19(2):57–62
Vijayalakshmi U, Rajeswari S (2012) Influence of process parameters on the sol–gel synthesis of nano hydroxyapatite using various phosphorus precursors. J Sol-Gel Sci Technol 63:45–55
Vollmer N, Ayers R (2012) Decomposition combustion synthesis of calcium phosphate powders for bone tissue engineering. Int J Self-Propag High-Temp Synth 21(4):189–201
Webster TJ, Ergun C, Doremus RH, Siegel RW, Bizios R (2000) Enhanced functions of osteoblasts on nanophase ceramics. Biomaterials 21(17):1803–1810. https://doi.org/10.1016/s0142-9612(00)00075-2
Westheimer FH, Huang S, Coritz F (1988) Rates and mechanisms of hydrolysis of esters of phosphorus acids. J Am Chem Soc 110:181–185
Wu SC, Tsou HK, Hsu HC, Hsu SK, Liou SP, Ho WF (2013) A hydrothermal synthesis of eggshell and fruit waste extract to produce nanosized hydroxyapatite. Ceram Int 39:8183–8188. https://doi.org/10.1016/j.ceramint.2013.03.094
Yang F, Jin C, Subedi S, Lee CL, Wang Q, Jiang Y, Li J, Di Y, Fu D (2012) Emerging inorganic nanomaterials for pancreatic cancer diagnosis and treatment. Cancer Treat Rev 38:566–579. https://doi.org/10.1016/j.ctrv.2012.02.003
Yuvaraj S, Fan-Yuan L, Tsong-Huei C, Chuin-Tih Y (2003) Thermal decomposition of metal nitrates in air and hydrogen environments. J Phys Chem B 107:1044–1047. https://doi.org/10.1021/jp026961c